J Comput Neurosci (2009) 26:109–118
DOI 10.1007/s10827-008-0101-y

Stereotactic model of the electrical distribution within the internal globus pallidus during deep brain stimulation

Xavier Vasques · Laura Cif · Olivier Hess · Sophie Gavarini · Gerard Mennessier · Philippe Coubes

Received: 31 January 2008 / Revised: 7 April 2008 / Accepted: 16 May 2008 / Published online: 17 June 2008

Abstract Deep brain stimulation (DBS) of the internal globus pallidus (GPi) is an established surgical technique for the treatment of movement disorders. The objective of this study was to propose a computational stereotactic model of the electrical distribution around the electrode within the targeted GPi in order to optimize parameter adjustment in clinical practice. The outline of the GPi can be defined precisely by using stereotactic magnetic resonance imaging (MRI) and from this it is possible to model its three-dimensional structure. The electrode and the distribution of the patient-specific parameters can then be co-registered with the GPi volume. By using this methodology, it is possible to visualize and measure the relationship between the electrical distribution of patient-specific parameters and the morphology of the GPi. The model could be applied in clinical practice to help determine the threshold for achieving a therapeutic effect and consequently may aid in optimizing parameter settings for individual patients.

Keywords Computational stereotactic model · Deep brain stimulation · Internal globus pallidus · Electrical distribution · MRI-based · Movements disorders

Action Editor: Charles Wilson

X. Vasques · L. Cif · S. Gavarini · P. Coubes (✉)
CHRU Montpellier, Service de Neurochirurgie,
Hôpital Gui de Chauliac,
Unité de Recherche sur les Mouvements Anormaux,
80 Avenue Augustin Fliche,
34295 Montpellier Cedex 05, France
e-mail: p-coubes@chu-montpellier.fr

X. Vasques · L. Cif · S. Gavarini · P. Coubes
IGF, Montpellier 34094,
France

X. Vasques · L. Cif · S. Gavarini · P. Coubes
CNRS UMR5203,
Montpellier 34094, France

X. Vasques · L. Cif · S. Gavarini · P. Coubes
INSERM, U661,
Montpellier 34094, France

X. Vasques · L. Cif · S. Gavarini · P. Coubes
Université Montpellier I,
Montpellier 34094, France

G. Mennessier
Laboratoire de Physique Théorique et Astroparticules,
UMR CNRS 5207, Université Montpellier II,
Montpellier, France

O. Hess
Deep Computing Europe,
IBM Montpellier,
Montpellier, France

1 Introduction

Deep brain stimulation (DBS) of the basal ganglia represents an effective surgical technique for the treatment of movement disorders, notably Parkinson's disease (PD; Benabid et al. 2005) and dystono-dyskinetic syndromes (DDS; Coubes et al. 1999; Coubes et al. 2000; Coubes et al. 2004; Krauss et al. 2003). Numerous studies have examined the use of DBS in treating other neurological disorders including epilepsy (Hodaie et al. 2002) and multiple sclerosis (Wishart et al. 2003), as well as psychiatric disorders including depression (Mayberg et al. 2005) and obsessive compulsive disorder (Nuttin et al. 2003). Continuous bilateral electrical stimulation of the internal globus pallidus (GPi) is now a commonly used treatment for DDS. A wide range of factors can influence outcome including

clinical, surgical and electrical variables. To date, selection of stimulation parameters (i.e. contact configurations, frequency, pulse width and voltage) during follow-up is time consuming and based on clinical observation and physician experience. One way to establish optimal parameters could be to measure and visualize them in the context of the anatomy of each individual patient.

The surgical protocol developed in our center for locating the anatomical target includes pre- and postoperative magnetic resonance imaging (MRI) with a Leksell Frame under general anaesthesia (Coubes et al. 2002). This procedure have been shown to have a very low complication rate (Vasques et al. 2008; 0% bleeding) and to be highly precise (Hariz 2002; Coubes et al. 2002; Vayssiere et al. 2000). The objective of the present study was to propose a computational anatomical model based on stereotactic MRI coupled with an electrical distribution model of DBS [i.e. isopotential (ISP), isofield (ISF) and current density] that can be applied both pre- and postoperatively to patients already implanted, in the most controlled environment possible. Thus, the model aims to optimize target localization at the time of surgical planning, allowing electrode localization after surgery and adjustment of electrical parameters in clinical practice. The model could also facilitate volumetric studies of target nuclei in movement disorders.

With this aim in mind, we decided to monitor stereotactic points along the edges of the GPi directly on MRI (Starr et al. 1999). These coordinates were then used to build up a 3D model of the GPi, allowing calculation of the volume of the target. The target volume could then be correlated with the electrical parameters which were recorded from the internal pulse generator (IPG) during stimulation. This methodology allowed the individual structural spatial variations between patients to be taken into account. Electrical field values were correlated with the GPi anatomy in one reference patient.

2 Materials and methods

2.1 Electrical distribution: theoretical model

Subsequent to the design of the 2D-electrical field model (Hemm et al. 2005), a three-dimensional model of the *in vivo* stimulation system was developed which included the lead (four contacts numbered from 0 to 3, radius: 0.635 mm, electrodes height: 1.5 mm, separation: 0.5 mm; ref: 3389, Medtronic, Reuil-Malmaison, France) and the IPG (Model 7424, 7425, 7426, Medtronic).

Brain tissue in the vicinity of the stimulating lead was assumed to be isotropic and homogeneous due to the low density of neurons in the GPi (Yelnik 2002) compared to other structures including the subthalamic nucleus (STN). The brain tissue around the lead was represented by a cylinder (with a radius of 40 mm and a height of 80 mm). The size of the cylinder was determined by the electrical field strength at its boundary. The maximum electrical field strength on the boundaries for monopolar stimulation is ~0.001 V/mm depending on the voltage used and which contacts are activated.

The height of the cylinder was calculated from the mean length of the trajectory from the entry point on the cortical surface to optic tract (on the inferior surface of the brain). Calculations demonstrate that this value was necessary and sufficient because superior values do not modify the final result. Different stimulation modalities were applied: monopolar stimulation with single or multiple electrodes activated to serve as the negative pole (with the IPG serving as the positive pole); and bipolar, in which the current flows between two or more electrodes. The borders of the cylinder were considered to be insulators in the bipolar mode. In the monopolar mode, the IPG was modelled as an additional perfect conductor disk with a radius of 20 mm located at the bottom of the cylinder. The DBS model displays and calculates the electrical current distribution from the patient's electrical parameters recorded by telemetry. Furthermore, the software allowed the electrical distribution within the GPi to be displayed preoperatively by using theoretical impedance values. The radius of the modelled IPG was calculated by comparing and adapting the magnitude of the ratios of impedances in monopolar and bipolar modes in the model to the mean values measured in patients using the Medtronic radiofrequency console programmer. Preoperatively, the model impedance is representative of the clinical impedance (For example, contact 1 as negative pole: 1,185 Ω, contact 1 and 2 as negative poles: 811.6 Ω, contact 1 as negative pole and contact 2 as positive pole: 1,478.8 Ω).

Possible interactions between the two implanted electrodes in bilateral stimulation were not taken into account.

The distribution of the potential $U(r, z)$ was determined as the solution of the Laplace equation where r represents the radius and z is the distance in height from the middle of the lead. The Laplace equation was reduced in cylindrical coordinates according to the axial symmetrical model:

$$\frac{1}{r}\frac{\partial}{\partial r}\left(r\frac{\partial U}{\partial r}\right)+\frac{\partial^2 U}{\partial z^2}=0 \qquad (1)$$

Boundary conditions were defined according to given potentials imposed at the metal contacts (depending on the specific mode of stimulation) and to zero values of the normal electrical field component (En=−dU/dr) at the insulating surfaces of the central electrode and of the external cylinder. The latter condition is a direct consequence of the requirement that the component of the current density, normal to the

surface of an insulator, is zero. The non-stimulated contacts are electrical conductors that can thus present a non-zero potential. The initial value for these contacts is an unknown constant potential to be determined from the fact that the total current is zero. A finite differences method was used for numerical analysis. An analytical description near the metallic edges was incorporated into the finite-difference scheme. The space step size is variable; it is smallest near the electrode and largest near the cylinder. For example, the distance between successive points near the contact is ~0.05 mm (z and r), whereas it is ~1 mm (z and r) near the cylinder. The singularities near the extremities of the contacts were approached by a Taylor dominant order expansion (order= 0). The electrical field and the current density were deduced from the potential.

The stimulus waveform generated by the Medtronic IPG is biphasic, and the technical amplitude of the stimulus waveform is defined by the peak-to-peak voltage of the cathodic and anodic phases (Butson and McIntyre 2007). The true stimulus waveform generated by the Medtronic IPG was used rather than the amplitude registered on the clinical programmer in order to improve the accuracy of the DBS model. The stimulation waveforms of the electrical settings currently used in our center were recorded from the Soletra IPG on a digital storage oscilloscope (Tektronix, France) and the results were integrated on the computer program. The measurements were comparable with those of the Butson and McIntyre study (Butson et al. 2007).

2.2 Stereotactical GPi: theoretical model

The stereotactic protocol used for the localization of the anatomical target in our centre involves a pre- and postoperative stereotactic 1.5-T MRI (slice thickness of 1.5 mm for both T1- and T2-weighted images) under general anaesthesia (Coubes et al. 2002). The efficacy and reproducibility of the therapy are based on a precise delineation of the GPi borders (Vayssiere et al. 2000; Vayssiere et al. 2002).

In line with our experience in movement disorder surgery, based on direct MRI targeting of the GPi (478 electrodes implanted in 220 procedures: 426 for dystono-dyskinetic syndromes and 52 for Parkinson's disease), we sought to model the GPi by selecting real points on structural borders in axial, sagittal and coronal planes. This was performed by the neurosurgeon who directly identifies on MRI, the points of highest contrast located exactly at the limit of the targeted structure. The neurosurgeon decided where the target finished and pinpointed the pixel considered as being at the interface between the target and the surrounding brain with certitude (Fig. 1). The points were expressed using the Leksell reference system, without reference to an atlas.

These points, called "points of certainty" or "C-points", allowed a 3D model of the GPi (Fig. 1) to be built by using implicit surface representation (Blinn 1982). The first step in building the GPi contours was to determine the implicit equation of the surface formed by scattered points. The GPi surface was created by using a linear combination of radial basis functions (Morse et al. 2001). The use of compactly supported radial basis functions reduces the method execution time. The implicit equation representing the surface is defined as a linear combination of these basis functions:

$$F(x) = \sum_{i=1}^{n} d_i \times \Phi(\|\bar{x} - \overline{x_i}\|) = 1 \tag{2}$$

where $\overline{x_i}$ is the position of the known values, the weights d_i are coefficient values to be determined and Φ is the basis functions. The goal is to determine the weights d_i such that $\forall_i \in (1,n), F(\overline{x}_i) = 1$.

Solving the equation for the weights d_i and denoting $\Phi_{ij} = \Phi\left(\left\|\overline{X_i} - \overline{X_j}\right\|\right)$ produces the following system:

$$\begin{bmatrix} \Phi_{11} & \Phi_{12} & \dots & \Phi_{1n} \\ \Phi_{21} & \Phi_{22} & \dots & \Phi_{2n} \\ \vdots & \vdots & \ddots & \vdots \\ \Phi_{n1} & \Phi_{n2} & \dots & \Phi_{nn} \end{bmatrix} \begin{bmatrix} d_1 \\ d_2 \\ \vdots \\ d_n \end{bmatrix} = \begin{bmatrix} 1 \\ 1 \\ \vdots \\ 1 \end{bmatrix} \tag{3}$$

A basis function was chosen to give a more accurate model of the grey nuclei, notably the GPi, because of the low number and the unorganized nature of the stereotactic points surrounding the GPi (total points ~50) that were selected by the physician. This function is represented below:

$$\Phi_i(x,y,z) = \left(1 - \frac{d}{R}\right)2 \tag{4}$$

where $d = \sqrt{(x-x_i)^2+(y-y_i)^2+(z-z_i)^2}$, ($x_i$, y_i, z_i) are the stereotactic coordinates, and R is an adjusted radius constant. The first step in order to determine the radius is to calculate the coordinates of the center of gravity of the GPi (cgx, cgy, cgz). The x coordinate of the stereotactic point that is at the *maximum* distance from the center of gravity of the GPi ($X_{\max}$) and the y coordinate of the stereotactic point at the *minimum* distance from the center of the gravity of the GPi ($Y_{\min}$) are then determined. The R value was described by the following expression:

$$R = 110 \times \frac{(X_{\max} - cgx) - (Y_{\min} - cgy)}{\sqrt{\text{Number of stereotactic points}}}$$

The system Eq. (3) was solved by using the LU factorization. Once the weights d_i had been determined,

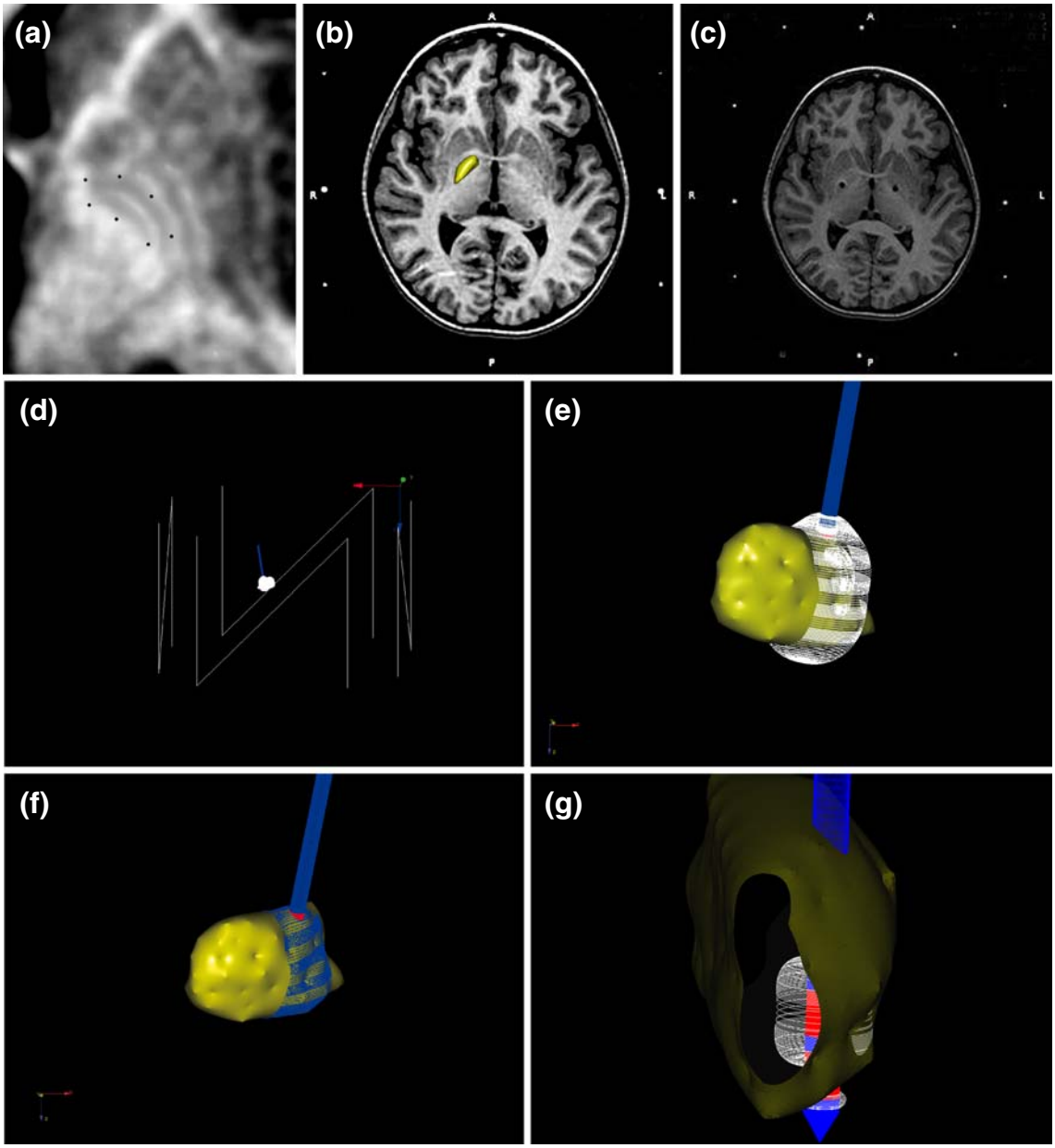

Fig. 1 Correlation of the anatomical and electrical data in an illustrative case, a 12 year-old girl with severe primary DYT1 dystonia whose symptoms resolved after bilateral DBS. (**a**) An illustrative MRI showing the definition of the C-points. (**b**) The anatomical GPi model overlaid on the preoperative MRI. (**c**) Stereotactic axial MR imaging slice passing through the target. (**d**) Posterior view of the GPi, the lead, the electric field within the 3D stereotactic frame showing the origin of the coordinate system. (**e**) Isofield lines from 0.025 to 1 V/mm within the sensory-motor part of the GPi. (**f**) The blue hatching represents the volume of intersection between the $ISF_{0.025}$ line and the left GPi. (**g**) Extrapolation of an isofield line value showing the correlation between the GPi and the electric field value 0.2 V/mm in an illustrative case (contact 1 negative, 1.3 V, 1,185 Ω)

the implicit equation could then define the surface to be reconstructed.

2.3 Correlation between electrical parameters and GPi anatomy

The theoretical models were computed by using a C/OpenGL computer program that applies the Marching Cubes algorithm of Lorensen and Cline (Lorensen and Cline 1987).

Two steps were required for correlating the anatomical information with the electrical distribution in a given patient. Firstly, C-points and target coordinates including the trajectory angles were registered on the software. Secondly, the electrical parameters of the lead were selected for each patient and were then recorded from the IPG, in order to visualize, manipulate and measure the correlation between the electrical distribution and the GPi anatomy of the patient. The software displayed an interface where the

electrical settings of the lead could be changed (voltage, electrode configuration and impedance). It was possible to extrapolate the line representing a specific ISF value (or ISP value or current density value) from a group of lines (from 0 to 1 V/mm) and to calculate its surface area and the volume enclosed within it. Zoom, translation and rotation tools were also implemented.

2.4 Clinical application

This method was applied to data recorded from a 12-year-old female patient, utilizing postoperative MRI data indicating the anatomical information, the target coordinates and the trajectory angles. The follow-up period was 2 years. The patient presented with severe genetic primary DYT1 dystonia and underwent surgery for bilateral postero-ventral GPi lead implantation. Dystonic symptoms were assessed pre- and postoperatively at pre-determined intervals using the Burke–Marsden–Fahn dystonia rating scales (BMFDRS; Burke et al. 1985). Continuous bilateral stimulation was applied with the following settings: monopolar mode with electrode 1 as negative and, the IPG as positive, a rate of 130 Hz, a pulse width of 450 μs, and a voltage of 1.1 volts (V). The settings were then adapted according to the clinical response (Table 1). Given the parameters of the model and the electrode configuration of the patient (contact one as a negative pole), preoperatively, the calculated model impedance is 1,185 Ω.

The volumes stimulated by each ISF line were studied at 3 and 24 months. Thereafter, three ISF values were compared more specifically: 0.1, 0.2 and 0.4 V/mm.

3 Results

3.1 Clinical practice: electrical parameter distribution in the GPi anatomy of the patient

Application of this model to the present study has been possible using standard PCs, with several working systems. The compilation and execution of the program take 1 min and 45 s for visualization with a grid of 256×256×256 (6 s with a 100×100×100 grid), without taking into account the time necessary to define the C-points on MRI (which is operator dependant). The surface was defined with a mathematical curve representing the GPi which could be calculated at different levels of detail by increasing the size of the grid. Preoperatively, the software allowed the display of the electrical distribution within the GPi of the patient by using theoretical impedance. The display and calculation of the surface and volume of both the GPi and the intersection between the electrical distribution and the GPi were possible (Fig. 1) i.e. the intersection between the volume of each electrical field value and the GPi volume. In clinical practice, taking into account the patient electrical parameters recorded by telemetry, the physician can thus visualize, manipulate and calculate the electrical distribution around the DBS lead in the anatomy of patients.

3.2 Influence of the electrical settings on the stimulated volume

For a given voltage, the shape and volume of the ISF, ISP and current density line distribution varies greatly between monopolar and bipolar configuration (Fig. 2). For a voltage of 1.1 V registered on the clinical programmer, the isofield lines 0.1 V/mm ($ISF_{0.1}$) had a volume of 40.9 mm^3 in the monopolar mode (electrode 1 negative), and 54.7 mm^3 in the bipolar mode (electrodes 1 and 3 positive, electrode 2 negative). When the voltage was increased to 1.5 V on the clinical programmer, the volume of the $ISF_{0.1}$ was 67.7 mm^3 in monopolar mode and 72.8 mm^3 in bipolar mode.

3.3 Application to a specific case

Electrical field distribution was correlated with the patient's anatomy by using the postoperative stereotactic MRI, which gave the anatomical information, the target coordinates and the trajectory angles of the leads.

The volumes of the GPi were 629.7 mm^3 on the right and 596.3 mm^3 on the left (Fig. 3). An increase in the

Table 1 Clinical scores, functional scores (BMFDRS) and electrical settings of a patient treated by DBS

	Preoperative	3 months postoperative	2 years postoperative
Clinical score (/120)	42	26	4
Functional score (/30)	14	14	2
Parameter settings on the left system	–	Electrode 1−, case+, 1.1 V (measured amplitude 1 V), 62 μA 1,208 Ω	Electrode 1−, case+, 1.5 V (measured amplitude 1.34 V), 2 μA 1,848 Ω
Parameter settings on the right system	–	Electrode 1−, case+, 1.1 V, 49 μA 1,505 Ω	Electrode 1−, case+, 1.3 V, 45 μA 1,840 Ω

Given the parameters of the model and the electrode configuration of the patient, the theoretical impedance calculated is 1,185 Ω.

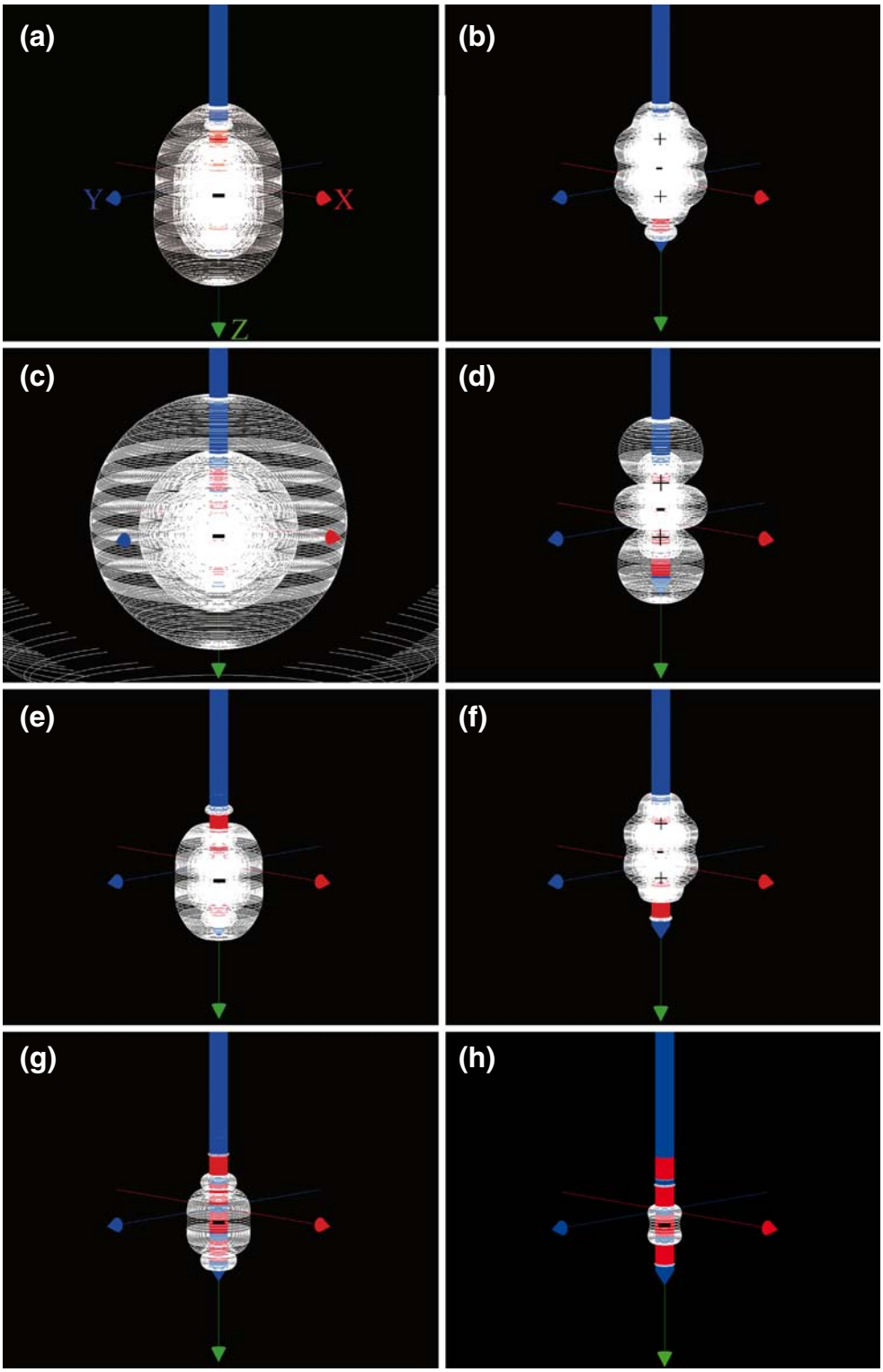

Fig. 2 Distribution of the electrical parameters around the electrode represented by the isofield (**a**, **b**), isopotential (**c**, **d**) and current density (**e**, **f**) lines. The stimulation parameters that were used included electrode 1 negative, case positive, 1.1 V (**a**, **c**, **e**, **g**, **h**) and electrode 1 and 3 positive, electrode 2 negative, 1.1 V (**b**, **d**, **f**). The insulator of the lead is represented in blue and the electrodes in *red*. The isofield lines are visualized every 50 mV/mm (from 0.025 to 1 V/mm) and the isopotential lines are visualized every 50 mV. The isofield line of 0.1 V/mm (volume of 55.5 mm^3) and 0.4 V/mm (volume of 6.4 mm^3) have been extrapolated (**g** and **h**). By default the conductivity is 0.1 $\Omega\ m^{-1}$. However, the conductivity is modified when changing the impedance, influencing the current density

stimulated volume up to a certain level, achieved by increasing the voltage, induced a clinical improvement in this patient. From month 3 to month 24, only the $ISF_{0.025}$ and $ISF_{0.05}$ lines reached the postero-medial border of both sides of the GPi. With the configuration settings used at 3 months (Table 1), the postero-lateral part of the GPi was only reached by the ISF lines from 0.025 to 0.350 V/mm (from 0.375 to 1 V/mm inside the GPi) on the right side and from 0.025 to 0.3 V/mm on the left side.

At 2 years of follow-up, with an improvement of more than 90% in the clinical part of the BMFDRS, the ISF lines from 0.025 to 0.4 V/mm reached the postero-lateral part of

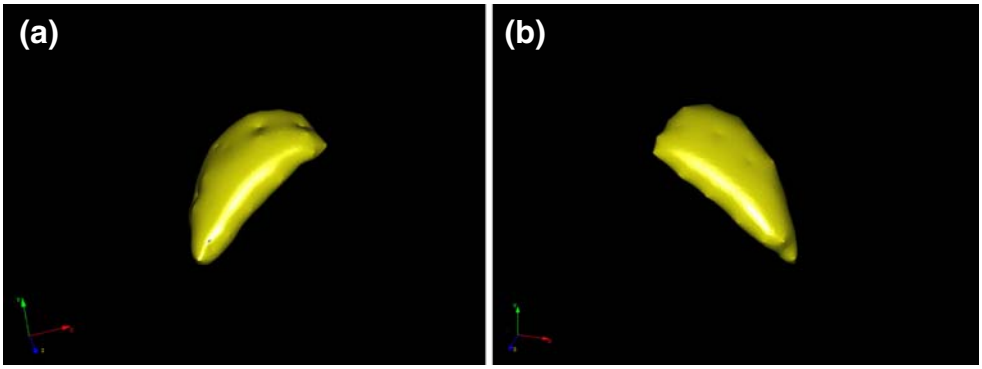

Fig. 3 Both GPi of the patient with a 256×256×256 grid. The volumes of the GPi were 629.7 mm^3 on the *right side* (**a**) and 596.3 mm^3 on the *left side* (**b**)

the right GPi and from 0.025 to 0.425 V/mm on the left GPi.

Three electric field values were compared more specifically: $ISF_{0.1}$, $ISF_{0.2}$ and $ISF_{0.4}$ (Fig. 2).

At 3 months, on the right side, the volume intersections (and surface intersections) with the GPi were 35.5 mm^3 (22.6 mm^2), 18.7 mm^3 (4.4 mm^2) and 6.38 mm^3 (0 mm^2) respectively (Fig. 4). The $ISF_{0.4}$ was completely within the GPi. The postero-lateral part of the GPi was reached by the $ISF_{0.1}$ and $ISF_{0.2}$ and no electric field value reached the postero-medial section. Similar results were obtained for the left GPi.

At 24 months, on the right side, the volume intersection (and surface intersection) with the GPi was 58.4 mm^3 (22.8 mm^2), 20.5 mm^3 (7.29 mm^2) and 10.35 mm^3 (1.39 mm^2) respectively (Fig. 4). In contrast to the electrical parameters at 3 months, the $ISF_{0.4}$ reached the postero-lateral border of the GPi. The lateral part of the GPi was also reached by the $ISF_{0.1}$ and $ISF_{0.2}$ and no electrical field value reached the postero-medial section. There were no significant changes in the left GPi.

4 Discussion

The objective of this study was to develop a computational MRI-based stereotactic anatomical model coupled with a DBS model in order to aid surgical planning, contact

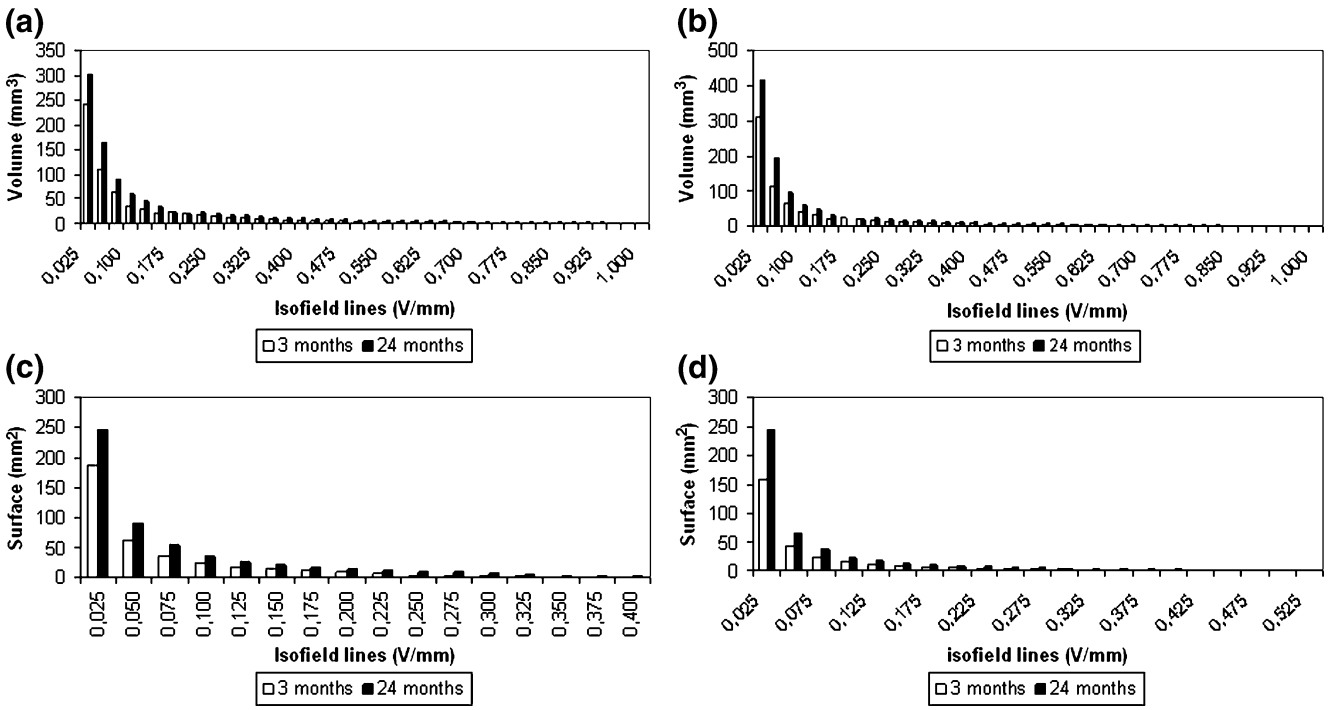

Fig. 4 Volume (**a**, **b**) and surface (**c**, **d**) measurements of the correlation between the isofield lines and the GPi of the DYT1 patient with parameters at months 3 and 24. (**a**) Intersection of the isofield lines volume and the right GPi volume. (**b**) Intersection of the isofield lines volume and the left GPi volume. (**c**) Surface intersection of the isofield lines and the right GPi surface. (**d**) Surface intersection of the isofield lines and the left GPi surface

localization after surgery and parameter adjustments during the course of DBS.

4.1 GPi model

It is a commonly used technique in MRI studies to depict the outlines of structures of interest on brain slices and then to digitize them to create a stack of contours. Promising segmentation (automatic or manual) and energy minimization methods exist for modelling the basal ganglia. However, segmentation from MR images remains difficult because of the low levels of contrast and the absence of easily visible contours due to unstable anatomical limits between structures. Segmentation of the ventricular system can be performed relatively easily because there is a definite contrast between cerebrospinal fluid and the surrounding brain (Colliot et al. 2006; Ciofolo and Barillot 2005; Collins et al. 1995). However, up to now, segmentation of grey nuclei including caudate nuclei, thalami and GPi, the surgical target in DDS, seems to be more difficult. These difficulties are anatomically determined by the small size of the structures, and the heterogeneity and irregularity of their interfaces with the surrounding white matter. Particularly in the case of a disorder secondary to a lesion seated in the grey nuclei, their shapes can be irregularly modified and there is also a lower level of contrast between structures (similar histological structures). Segmentation methods commonly use atlases (Bloch et al. 2003; Xue et al. 2001) and deformable templates (Pitiot et al. 2004) based on statistical shape training. The drawback of these techniques is the inter-individual anatomical variation which has major impact on the final precision. This inter-individual variation has been studied previously (Vayssiere et al. 2002). The differences between the target coordinates obtained with direct visualization by MRI and those based on atlases prompted the present study. The actual location of the target might differ significantly from the theoretical statistical target location due to individual variation. The advantage of the approach put forward here is that the individual anatomy of the patient is taken into account for the surgical planning. Each C-point can be localized within the stereotactic frame by direct visualization of its coordinates under visual control, which is an important feature of this model compared to previously published models. The resulting unorganized collection of scattered data points allows a semi-automated reconstruction of the GPi surface under visual control. Field-based implicit surface methods have become increasingly popular in recent years with Blobby Molecules (Blinn 1982), *R*-functions (Pasko et al. 1995) and convolution surfaces (Bloomenthal and Shoemake 1991), all with different applications: shape morphing, natural phenomena simulation and space deformation. The method used in this study for interpolating the scattered points was chosen because of its robustness when scattered points are non-uniform. The interpolation of the implicit surface using compactly supported radial basis functions (Morse et al. 2001) was appropriate for generating the complex organic shapes and has an advantage in terms of computational expense.

4.2 Electrical field distribution in the GPi anatomy of the patient: analysis and limitations

One limitation of this study is the use of a homogenous model. Many groups use anisotropic brain models, which take into account the grey/white matter distribution and fibre direction using diffusion tensor imaging (DTI) to try to understand the mechanisms of action of DBS (Butson et al. 2007; McIntyre et al. 2004; Miocinovic et al. 2006). Tissue inhomogeneities such as small lacunar cavities can modify the shape of the electric field distribution (Astrom et al. 2006; Butson et al. 2007). McIntyre et al. (McIntyre et al. 2004) described a neural model for subthalamic nucleus (STN) stimulation. They determined the conductivities of the STN from diffusion tensor magnetic resonance data in one patient and correlated them with neuron cable models taking into account axon diameter and internodal spacing. This model (McIntyre et al. 2004) gives a more faithful representation of real brain structures by reflecting the heterogeneity of the STN. Aström et al. (Astrom et al. 2006) studied the effects of cystic cavities on electrical field distribution in the GPi by modelling a grey matter nucleus with and without cerebrospinal fluid filled cystic cavities to mimic Virchow–Robin perivascular spaces (VRPS). The GPi and the VRPS were modelled as spheres and not in their irregular shapes. Butson et al. (Butson et al. 2007) developed a patient-specific model of STN for Parkinson's disease to predict the volume of tissue activated by DBS. The model showed that the volume of tissue activated by DBS differs between isotropic and diffusion tensor MRI. These approaches are promising because they take into account the heterogeneity of the brain. Their model gives an important indication of how the surrounding structures may influence the shape of the electrical field and subsequent neural response to stimulation.

Up to now, even though highly specific, models using DTI are difficult to apply to neurosurgical and clinical practice where individual brain anatomy is the most important factor. The precision of the surgical procedure is an issue of major importance given the submillimeter accuracy of lead insertion needed to hit the target. DTI is not currently appropriated due to limited image resolution. An accurate measurement of small structures or interfaces between structures like GPi/GPe requires high spatial resolution, but high submillimeter DTI cannot be currently achieved. To create a model using DTI, it is necessary to

use multiple image co-registration and atlas representations which involve spatial variability and increase the time of surgery. Furthermore, DTI could not be applied to the entirety of our population already implanted with a DBS system (Vasques et al. 2008). In this study, the risk of error due to multiple image co-registration and anatomical variability has been limited by using the stereotactic coordinates of targets selected directly on MRI. The model can also be applied in routine clinical practice in patients who already have a DBS system implanted by using the postoperative stereotactic MRI and the electrical parameters recorded by telemetry. Preoperatively, the model allows the display and the calculation of the electrical distribution within the GPi of the patient using theoretical impedance. Based on the evaluation of the *in vivo* impedance and current values measured in patients (Hemm et al. 2004), the theoretical impedance seems to be an acceptable approximation for the preoperative surgical planning. Hemm et al. (Hemm et al. 2004) showed that for patient with a greater than 80% improvement on the BFMDRS, the mean impedance with a single contact activated as the negative pole is 1,283±215 Ω; close to the calculated impedance in our model (1,185 Ω). However, prediction of impedance preoperatively is difficult because the electrical brain impedance of each individual patient is unique (Hemm et al. 2004). Given the model parameters and the electrode configuration of the patient in the present study at 3 months, the calculated impedance is 1,185 Ω, which is close to the recorded impedance on the left side (1,208 Ω) and differs from the recorded impedance on the right side (1,505 Ω) by 420 Ω. Preoperatively, depending on the impedance for a given patient, the results may represent an overstimulation of the stimulated volume.

For the purposes of this study, the brain tissue in the vicinity of the stimulating lead was assumed to be homogeneous and to have an isotropic resistance due to the low density of neurons in the GPi compared with the STN (Yelnik 2002). This would seem to be acceptable especially if it is assumed that only the ISF lines within the GPi have a therapeutic effect. It has been reported that the most effective position for the lead is in the posterior, medial and ventral part of the GPi (Coubes et al. 2002; Tisch et al. 2007); This has been shown to be the sensorimotor area (Laitinen et al. 1992) and close to the output pathway i.e. the ansa lenticularis. If these fibres must be stimulated to obtain optimum therapeutic effect, it can be concluded that these fibers must be within the volume to be stimulated. The GPi somatotopic organization (Vayssiere et al. 2004) favours the hypothesis that different neuron populations within the GPi are responsible for the control of different body parts. These populations would be organized in several fascicules rather than a single one containing all output fibres. The actual target is a network-specific target probably influencing remote structures and representing only a subsection of the stimulated volume. The application of the model to one clinical case indicates how this combination of electrical and anatomical information could be used to quantify the electric field necessary to produce the physiological effect. The activation of neurons is triggered by membrane depolarisation. This is due to a variation in the potential difference influenced by several factors including electrical and anatomical properties of neurons, distance and orientation relative to the electrode, tissue resistivities, stimulation waveform and configuration mode. The electrical field (voltage gradient parallel to the fiber) is probably the most important factor responsible for triggering the action potential because it varies with fiber orientation relative to the electrode. The visualization and quantification of specific isofield lines facilitates the determination of the stimulated region around the electrode. Depending on the position within the target, the trajectory angles of the lead, the patient electrical parameters, and the volume of the target and its morphology, an electric field value could emerge as the threshold value of the stimulated volume necessary to produce a therapeutic effect when applying this methodology to our entire population of patient with dystonia. For example, the electric field value of 1 V/mm can probably be considered to be insufficient as the resulting target (~1 mm width around the stimulated contact) seems too limited to be responsible for the clinical effect. In contrast, the value of 0.1 V/mm covers a large part of the GPi, even extending beyond the postero-lateral part of the GPi. We propose a method of modelling the electric field lines with the aim of identifying a threshold value and, consequently, the critical volume to be stimulated within the target to produce the optimum therapeutic effect. Its application to our dystono-dyskinetic patients in clinical practice could help to determine the threshold of the electrical field necessary to obtain a therapeutic effect, and possibly define the target as specifically as possible.

Acknowledgement This work was supported by grants from IBM France, Products and Solutions Support Center department (PSSC).

References

Astrom, M., Johansson, J. D., Hariz, M. I., Eriksson, O., & Wardell, K. (2006). The effect of cystic cavities on deep brain stimulation in the basal ganglia: a simulation-based study. *Journal of Neural Engineering*, *3*(2), 132–138.

Benabid, A. L., Chabardes, S., & Seigneuret, E. (2005). Deep-brain stimulation in Parkinson's disease: Long-term efficacy and safety—What happened this year? *Current Opinion in Neurology*, *18*(6), 623–630.

Blinn, J. F. (1982). A generalization of algebraic surface drawing. *ACM Transactions on Graphics*, *1*(3), 235–256.

Bloch, I., Géraud, T., & Maître, H. (2003). Representation and fusion of heterogeneous fuzzy information in the 3D space for model-based structural recognition application to 3D brain imaging. *Artificial Intelligence*, *148*, 141–175.

Bloomenthal, J., & Shoemake, K. (1991). Convolution surfaces. *Computer Graphics*, *25*(4), 251–256.

Burke, R. E., Fahn, S., Marsden, C. D., Bressman, S. B., Moskowitz, C., & Friedman, J. (1985). Validity and reliability of a rating scale for the primary torsion dystonias. *Neurology*, *35*(1), 73–77.

Butson, C. R., Cooper, S. E., Henderson, J. M., & McIntyre, C. C. (2007). Patient-specific analysis of the volume of tissue activated during deep brain stimulation. *NeuroImage*, *34*(2), 661–670.

Butson, C. R., & McIntyre, C. C. (2007). Differences among implanted pulse generator waveforms cause variations in the neural response to deep brain stimulation. *Clinical Neurophysiology*, *118*(8), 1889–1894.

Ciofolo, C., & Barillot, C. (2005). Brain segmentation with competitive level sets and fuzzy control. *Information Processing in Medical Imaging*, *19*, 333–344.

Collins, D. L., Holmes, C. J., Peters, T. M., & Evans, A. C. (1995). Automatic 3-D model-based neuroanatomical segmentation. *Human Brain Mapping*, *3*(3), 190–208.

Colliot, O., Camara, O., & Bloch, I. (2006). Integration of fuzzy spatial relations in deformable models—Application to brain MRI segmentation. *Pattern Recognition*, *39*, 1401–1414.

Coubes, P., Cif, L., El Fertit, H., Hemm, S., Vayssiere, N., Serrat, S., et al. (2004). Electrical stimulation of the globus pallidus internus in patients with primary generalized dystonia: Long-term results. *Journal of Neurosurgery*, *101*(2), 189–194.

Coubes, P., Echenne, B., Roubertie, A., Vayssiere, N., Tuffery, S., Humbertclaude, V., et al. (1999). Treatment of early-onset generalized dystonia by chronic bilateral stimulation of the internal globus pallidus. Apropos of a case. *Neuro-Chirurgie*, *45*(2), 139–144.

Coubes, P., Roubertie, A., Vayssiere, N., Hemm, S., & Echenne, B. (2000). Treatment of DYT1-generalised dystonia by stimulation of the internal globus pallidus. *Lancet*, *355*(9222), 2220–2221.

Coubes, P., Vayssiere, N., El Fertit, H., Hemm, S., Cif, L., Kienlen, J., et al. (2002). Deep brain stimulation for dystonia. Surgical technique. *Stereotactic and Functional Neurosurgery*, *78*(3–4), 183–191.

Hariz, M. I. (2002). Complications of deep brain stimulation surgery. *Movement Disorders*, *17*(Suppl 3), S162–S166.

Hemm, S., Mennessier, G., Vayssiere, N., Cif, L., El Fertit, H., & Coubes, P. (2005). Deep brain stimulation in movement disorders: Stereotactic coregistration of two-dimensional electrical field modeling and magnetic resonance imaging. *Journal of Neurosurgery*, *103*(6), 949–955.

Hemm, S., Vayssiere, N., Mennessier, G., Cif, L., Zanca, M., Ravel, P., et al. (2004). Evolution of brain impedance in dystonic patients treated by GPi electrical stimulation. *Neuromodulation*, *7*(2), 67–75.

Hodaie, M., Wennberg, R. A., Dostrovsky, J. O., & Lozano, A. M. (2002). Chronic anterior thalamus stimulation for intractable epilepsy. *Epilepsia*, *43*(6), 603–608.

Krauss, J. K., Loher, T. J., Weigel, R., Capelle, H. H., Weber, S., & Burgunder, J. M. (2003). Chronic stimulation of the globus pallidus internus for treatment of non-dYT1 generalized dystonia and choreoathetosis: 2-year follow up. *Journal of Neurosurgery*, *98*(4), 785–792.

Laitinen, L. V., Bergenheim, A. T., & Hariz, M. I. (1992). Leksell's posteroventral pallidotomy in the treatment of Parkinson's disease. *Journal of Neurosurgery*, *76*(1), 53–61.

Lorensen, W., & Cline, H. (1987). Marching cubes: A high resolution 3D surface construction algorithm. *Computer Graphics*, *21*(4), 163–169.

Mayberg, H. S., Lozano, A. M., Voon, V., McNeely, H. E., Seminowicz, D., Hamani, C., et al. (2005). Deep brain stimulation for treatment-resistant depression. *Neuron*, *45*(5), 651–660.

McIntyre, C. C., Mori, S., Sherman, D. L., Thakor, N. V., & Vitek, J. L. (2004). Electric field and stimulating influence generated by deep brain stimulation of the subthalamic nucleus. *Clinical Neurophysiology*, *115*(3), 589–595.

Miocinovic, S., Parent, M., Butson, C. R., Hahn, P. J., Russo, G. S., Vitek, J. L., et al. (2006). Computational analysis of subthalamic nucleus and lenticular fasciculus activation during therapeutic deep brain stimulation. *Journal of Neurophysiology*, *96*(3), 1569–1580.

Morse, B., Yoo, T., Rheingans, P., Chen, D., & Subramaniam, K. R. (2001). Interpolating implicit surfaces from scattered surface data using compactly supported radial basis functions. *Proceeding of the International Conference on Shape Modeling and Applications*.

Nuttin, B. J., Gabriels, L., van Kuyck, K., & Cosyns, P. (2003). Electrical stimulation of the anterior limbs of the internal capsules in patients with severe obsessive-compulsive disorder: Anecdotal reports. *Neurosurgery Clinics of North America*, *14*(2), 267–274.

Pasko, A., Adzhiev, V., Sourin, A., & Savchenko, V. (1995). Function representation in geometric modeling: Concepts, implementation and applications. *The Visual Computer*, *11*(8), 429–446.

Pitiot, A., Delingette, H., Thompson, P. M., & Ayache, N. (2004). Expert knowledge-guided segmentation system for brain MRI. *NeuroImage*, *23*(Suppl 1), S85–S96.

Starr, P. A., Vitek, J. L., DeLong, M., & Bakay, R. A. (1999). Magnetic resonance imaging-based stereotactic localization of the globus pallidus and subthalamic nucleus. *Neurosurgery*, *44*(2), 303–313.

Tisch, S., Zrinzo, L., Limousin, P., Bhatia, K. P., Quinn, N., Ashkan, K., et al. (2007). The effect of electrode contact location on clinical efficacy of pallidal deep brain stimulation in primary generalised dystonia. *Journal of Neurology, Neurosurgery, and Psychiatry*, *78*, 1314–1319.

Vasques, X., Tancu, C., Cif, L., Biolsi, B., Maldonado, I., Bonafe, A., et al. (2008). Cerebral Magnetic resonance imaging feasibility in patients with implanted neurostimulation system for deep brain stimulation. *The Open Magnetic Resonance Journal*, *1*(1), 1–8.

Vayssiere, N., Hemm, S., Cif, L., Picot, M. C., Diakonova, N., El Fertit, H., et al. (2002). Comparison of atlas- and magnetic resonance imaging-based stereotactic targeting of the globus pallidus internus in the performance of deep brain stimulation for treatment of dystonia. *Journal of Neurosurgery*, *96*(4), 673–679.

Vayssiere, N., Hemm, S., Zanca, M., Picot, M. C., Bonafe, A., Cif, L., et al. (2000). Magnetic resonance imaging stereotactic target localization for deep brain stimulation in dystonic children. *Journal of Neurosurgery*, *93*(5), 784–790.

Vayssiere, N., van der Gaag, N., Cif, L., Hemm, S., Verdier, R., Frerebeau, P., et al. (2004). Deep brain stimulation for dystonia confirming a somatotopic organization in the globus pallidus internus. *Journal of Neurosurgery*, *101*(2), 181–188.

Wishart, H. A., Roberts, D. W., Roth, R. M., McDonald, B. C., Coffey, D. J., Mamourian, A. C., et al. (2003). Chronic deep brain stimulation for the treatment of tremor in multiple sclerosis: Review and case reports. *Journal of Neurology, Neurosurgery, and Psychiatry*, *74*(10), 1392–1397.

Xue, J. H., Ruan, S., Moretti, B., Revenu, M., & Bloyet, D. (2001). Knowledge-based segmentation and labelling of brain structures from MRI images. *Pattern Recognition Letters*, *22*, 395–405.

Yelnik, J. (2002). Functional anatomy of the basal ganglia. *Movement Disorders*, *17*(Suppl 3), S15–S21.